PCCP

PAPER

View Article Online
View Journal | View Issue

Cite this: *Phys. Chem. Chem. Phys.*, 2015, **17**, 30119

Received 11th September 2015,
Accepted 19th October 2015

DOI: 10.1039/c5cp05437k

www.rsc.org/pccp

Hydrogen capture by porphyrins at the TiO_2(110) surface†

Giacomo Lovat,[ab] Daniel Forrer,[c] Mikel Abadia,[d] Marcos Dominguez,[ab] Maurizio Casarin,[e] Celia Rogero,[d] Andrea Vittadini*[c] and Luca Floreano*[a]

Metal-free porphyrin molecules adsorb on the rutile TiO_2(110) surface with their pyrrolic nitrogen atoms atop the O-bridge rows, whereas the iminic nitrogen atoms capture two additional hydrogen atoms. Hydrogenation occurs spontaneously at room temperature, irrespective of the distance of the polypyrrolic macrocycle from the surface, as varied by changing the porphyrin functionalization.

Introduction

Metal porphyrins (MPs) and phthalocyanines (MPcs) offer a large variety of electronic configurations that, when brought into contact with a substrate, can display the most diverse electronic and chemical functionalities,[1] spanning from magnetism[2] to catalysis.[3] In this context, the metal-free molecular homologues (2*H*-P and 2*H*-Pc) display large flexibility, as they can be suitably metalated *in situ* by post growth treatment, either by metal extraction from the substrate,[4] or by incorporation of diffusing adatoms (*e.g.* after atomic beam deposition).[5] Hydrogen itself can be exploited to modify the local molecular conductance by selective cleavage of one pyrrolic NH bond in 2*H*-P,[6] as well as tuning the chirality by selective adsorption in MnPc.[7]

In order to generalize these functionalities, one must take into account the nature of the substrate, which is demonstrated to affect the gas reactivity of the MP contact layer.[3c] The interface of titania with MPs and MPcs attracts large interest because of its dual purpose applications in photocatalysis and solar cells. In particular, the rutile TiO_2(110) surface is a suitable template for the growth of poly- and hetero-aromatic molecules thanks to its large and anisotropic surface corrugation. Phthalocyanine and porphyrin films are expected to grow with the molecular macrocycles closely parallel to the substrate,[5c,8–9] a geometry that favors intermolecular charge transport[10] and charge injection into the oxide substrate.[11]

A number of XPS measurements of different phthalocyanines and porphyrins grown on TiO_2(110) has however put in evidence the unexpected presence of pyrrolic nitrogen in metalated species, as well as an excess of pyrrolic nitrogen with respect to the iminic one in non-metalated molecules.[8,12–14] The nature of this component is controversial and has been alternatively attributed to chemical bonding of nitrogen to the oxygen atoms underneath,[8] or to a local surface screening effect,[12,14] or to hydrogen capture upon molecule de-metalation.[13] To better address this controversial issue we focused on the simplest case of metal-free porphyrins, which contain only two types of nitrogen atoms, namely pyrrolic and iminic. We performed experiments on three differently functionalized porphyrins: 2*H*-*tert*-butyl-tetra-phenyl-porphyrin (2*H*-TBTPP), 2*H*-tetra-phenyl-porphyrin (2*H*-TTP) and 2*H*-octa-ethyl-porphyrin (2*H*-OEP). These different peripheral terminations do not display specific (chemical) affinity for the substrate, and essentially change the height of the central macrocycle with respect to the surface by ~1 Å from 2*H*-TBTTP to 2*H*-OEP passing through the intermediate 2*H*-TPP.

Results and discussion

The ligand state of nitrogen in 2*H*-P can be probed by X-ray photoemission (XPS) measurements of the N 1s core level. Metal-free porphyrins are characterized by two well separated N 1s peaks of equal intensity (separation of ~2 eV), corresponding to one pair of hydrogenated (pyrrolic) nitrogen atoms and one pair of iminic (aza) nitrogen atoms.[15] However, the first layer molecules always display the occurrence of a dominant component at

[a] *CNR-IOM, Laboratorio Nazionale TASC, I-34149 Trieste, Italy. E-mail: floreano@iom.cnr.it*
[b] *Graduate School of Nanotechnology, University of Trieste, P.za Europa 1, I-34127 Trieste, Italy*
[c] *CNR-IENI and INSTM, via Marzolo 1, I-35131 Padova, Italy. E-mail: andrea.vittadini@unipd.it*
[d] *Materials Physics Center MPC, Centro de Física de Materiales (CSIC-UPV/EHU) and Donostia International Physics Center (DIPC), E-20018 San Sebastian, Spain*
[e] *Dipartimento di Scienze Chimiche, Università di Padova, via Marzolo 1, I-35131 Padova, Italy*

† Electronic supplementary information (ESI) available: Original NEXAFS data at the K-edge ionization threshold of C and N, XPS fitting analysis of N 1s, and computational details. See DOI: 10.1039/c5cp05437k

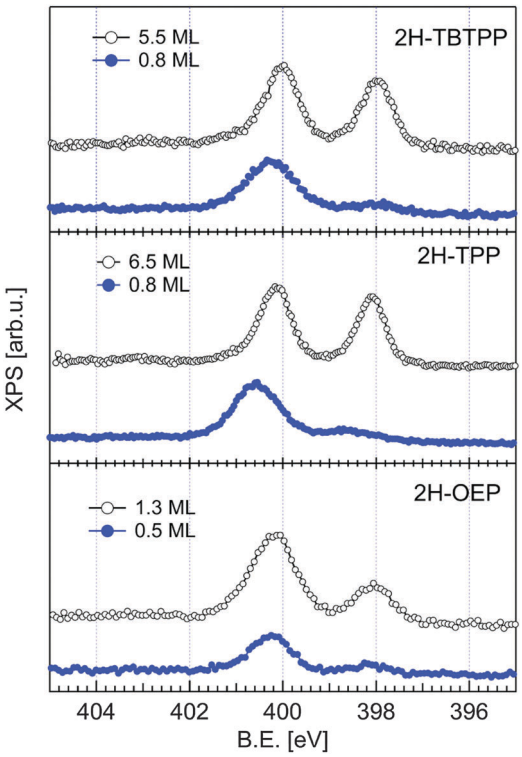

Fig. 1 Comparison between the monolayer (filled blue markers) and multilayer (open black markers) photoemission spectra of the N 1s peak for three different porphyrins ($h\nu$ = 500 eV; $\Delta E \sim 160$ meV). All films have been grown with the substrate at room temperature (RT). In the labels, the film thickness is indicated in monolayer, ML, units as defined by the first layer saturation coverage (see the Experimental section for details).

$\sim$400.2–400.5 eV in the N 1s photoemission spectra, as clearly shown in the bottom curves of Fig. 1 for 2*H*-TBTPP, 2*H*-TPP and 2*H*-OEP (from top to bottom). This binding energy corresponds to that of pyrrolic nitrogen, while the iminic component, which should display the same intensity as the pyrrolic one in the presence of regular porphyrins, is residual and is observed to increase only upon condensation of sequent layer molecules at $\sim$398 eV binding energy (see top curves of Fig. 1). We recall that also in metalated species, the four central nitrogen atoms become equivalent, but they yield a binding energy (BE) close to that of the iminic nitrogen atom (ΔBE $\sim$ +0.3 eV), without significant differences among different metal elements.

Concerning the molecular orientation, polarization dependent near-edge X-ray absorption spectroscopy (NEXAFS) at the K-edge of nitrogen and carbon always displays a large dichroism of the resonances associated with the pyrrolic rings (see Fig. S1 and S2, ESI†), which indicates that the three molecules are equivalently oriented with the central macrocycle almost parallel to the substrate. The main difference among the adsorption geometries of the molecules is thus the height of the macrocycle above the substrate (2*H*-TBTTP is $\sim$0.5 Å higher than 2*H*-TPP, which is $\sim$0.5 Å higher than 2*H*-OEP, from simple steric arguments and neglecting minor relaxation effects). This excludes that the absence of the iminic component in the N 1s spectra might be due a strong core level shift ($\sim$2–2.5 eV) of aza-nitrogen, originating either from local screening or by chemical bonding of nitrogen to the oxygen rows underneath. Rather, the local relaxation (tilting) of the phenyl rings in 2*H*-TPP might be responsible for the slightly larger binding energy (0.2–0.3 eV) with respect to 2*H*-OEP and 2*H*-TBTPP molecules, the terminations of which are likely less leaning to fit the substrate corrugation. We are then left with the hypothesis of hydrogen uptake, either molecular (from the vacuum residual gas) or atomic (from the substrate). In fact, a large and consolidated body of literature indicates that a significant amount of hydrogen is diluted in the TiO_2 bulk, as favored by thermal treatment, metal (acceptor) contaminants, and electron irradiation.[16] XPS is not a suitable probe of low concentration bulk-diluted species due to its intrinsic surface sensitivity (escape depth of 5–10 Å), however a few percent concentration of surface confined hydrogen species can be obtained by water dissociation at a slightly reduced TiO_2(110) surface.[17] These hydroxyl species can be easily monitored by photoemission of the valence band, where they give rise to a characteristic satellite of the O 2p band at $\sim$11 eV.[18]

In Fig. 2 we compare the valence band spectra of a clean, albeit slightly hydroxylated TiO_2(110) surface (estimated OH concentration of 4–5%) before and after the deposition of a layer of 2*H*-TPP, which is the intermediate height molecule. The hydroxyl peak is fully quenched upon molecular deposition in agreement with the hypothesis of hydrogen uptake. We remark that (i) full hydrogenation of nitrogen in the first porphyrin layer cannot be fulfilled only by the surface hydroxyls and (ii) the nitrogen hydrogenation is observed also in the absence of surface hydroxyls without any difference in the corresponding pyrrolic N 1s peak. This implies that either hydrogen is captured and dissociated from the residual gas pressure or that the porphyrin macrocycle locally lowers the kinetic barriers, which otherwise keep H interstitials in the subsurface region.

In order to further check the hypothesis of nitrogen hydrogenation, we performed *ab initio* calculations within the frame of gradient-corrected density functional theory (GGA-DFT) for the intermediate case of 2*H*-TPP (see computational details). Calculations predict that the gas-phase hydrogenation of 2*H*-TPP

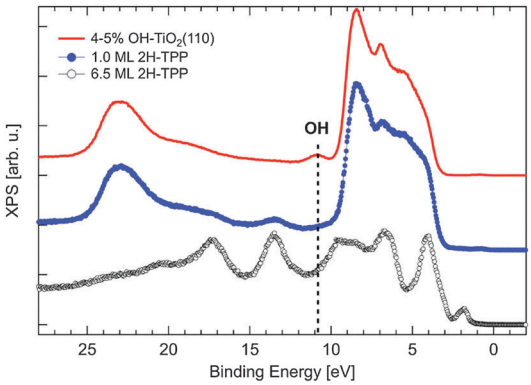

Fig. 2 Comparison between the extended valence band spectra ($h\nu$ = 140 eV; $\Delta E \sim 120$ meV) of a slightly hydroxylated TiO_2(110) surface before and after the deposition of 1.0 and 6.5 ML of 2*H*-TPP. The characteristic photoemission peak of the surface hydroxyls at BE $\sim$ 11 eV is completely quenched upon molecular deposition.

Table 1 Hydrogenation reaction energies

Reaction	ΔG [eV]
2*H*-TPP(gas) + H_2(gas) → 4*H*-TPP(g)	−0.10[a]
2*H*-TPP(ads) + 2H(ads) → 4*H*-TPP(ads)	−1.40[b]

[a] Zero-point energy corrections have been applied. [b] To avoid a lengthy study of the (weak) interactions among the adsorbed species, we assumed as the initial state two identical and separate slabs, one containing 2*H*-TPP(ads) and the other one containing two H atoms adsorbed at two (far) oxygen-bridge, O_{br}, atoms. As a final state, we instead considered two slabs representing 4*H*-TPP(ads) and a bare surface, respectively. See text for details about the structural configuration.

is slightly exothermic at 0 K (see Table 1), whereas, by assuming an ideal gas behavior for H_2, we can estimate that $\Delta G \approx +0.3$ eV at 298 K. This agrees with the fact that 2*H*-TPP, and not 4*H*-TPP, is the species stable at RT in the gas phase. At the same time, it strengthens the possibility that the TiO_2 substrate, which can provide dissociated hydrogen on the surface, favors the stabilization of the 4*H*-TPP species.

We then examined the case of absorbed 2*H*-TPP, using periodically repeated slab models with PBE-D theoretical lattice constants of the substrate.[19] In order to refine the configuration model of the adsorbed molecule, we performed scanning tunnelling microscopy (STM) measurements of a submonolayer coverage of 2*H*-TPP, where the N 1s spectra display the same CLS as the monolayer one (see Fig. S3, ESI†) and the uncovered substrate lattice can be easily recognized to determine unambiguously the 2*H*-TPP adsorption site.

As deposited at RT, all the molecules display a preferential adsorption configuration with a common azimuthal orientation. From the analysis of the STM images shown in Fig. 3, we can see that all molecules adsorb atop the oxygen rows with the squared molecular edge parallel to the substrate [001] direction. The individual molecules display a characteristic saddle-shape, which was reported also for 2*H*-TPP adsorbed on noble metals, and is originated by the opposite upward/downward tilt off the macrocycle plane of adjacent pyrrolic units. The corresponding nodal plane is oriented transverse to the oxygen rows and three distinct lobes can be distinguished on each side.

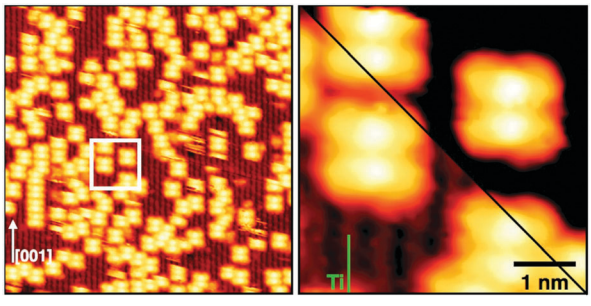

Fig. 3 Left: STM image (27.5 × 27.5 nm^2) of ∼1/3 ML of 2*H*-TPP deposited on the sample at room temperature (V_S = −1.5 V; I = 60 pA). The substrate Ti^{5f} (O_{br}) rows along the [001] direction appear as bright (dark) stripes. Right: Zoom in of the area indicated by the white square, as displayed with different contrast in order to highlight the molecular adsorption atop the dark O_{br} rows (bottom) and to enhance the intra-molecular structure (top).

Because of (i) the observed parallel to the surface orientation of the macrocycle (from NEXAFS dichroism) and (ii) the D_{2h} symmetric appearance of the molecules, we could limit our tests to two azimuthal orientations: with two opposite nitrogen atoms (N–N axis) oriented either along the substrate [001] direction or at 45° from it (see Fig. 4). We considered adsorption on both Ti 5-fold coordinated (Ti^{5c}) and oxygen-bridge 2-fold coordinated (O_{br} or O^{2c}) rows in both on-top and on-bridge sites (see Computational details). The most favored adsorption site for both 2*H*-TPP and its hydrogenated homologue 4*H*-TPP is found to be the bridge position between two adjacent O_{br} atoms along [001], with the N–N axis also parallel to the [001] direction. The resulting adsorption energies for the case of 4*H*-TPP are shown in Fig. 4, as computed for 3-layer slabs and large-core pseudopotentials.

The configurations parallel to the [001] direction (azimuth $\alpha = 0°$) and placed on O_{br} row sites are largely favored (∼1 eV) with respect to the other ones, the oxygen-bridge site being favored over the on-top one by ∼0.3 eV because of the stronger H-bond interaction. For 2*H*-TPP this difference is reduced to 0.2 eV because H-bonds are in general weaker. Our best estimates for adsorption energies, computed with 4 ML slabs and small-core pseudopotentials, are 5.31 eV and 3.41 eV for 4*H*-TPP and 2*H*-TPP, respectively.

We emphasize that in the most favored configuration two equivalent N–H···O_{br} hydrogen bonds are formed, as depicted in Fig. 5c; this configuration favors the downward tilt of the corresponding pyrrolic rings (Fig. 5a), whose peripheral carbon atoms protrude above the macrocycle plane and yield an enhanced intensity in the topographic images, as shown in the simulation of Fig. 5b. The other two central rings display a tilt in the opposite direction yielding a dimmed contrast in the direction transverse to the O_{br} rows.

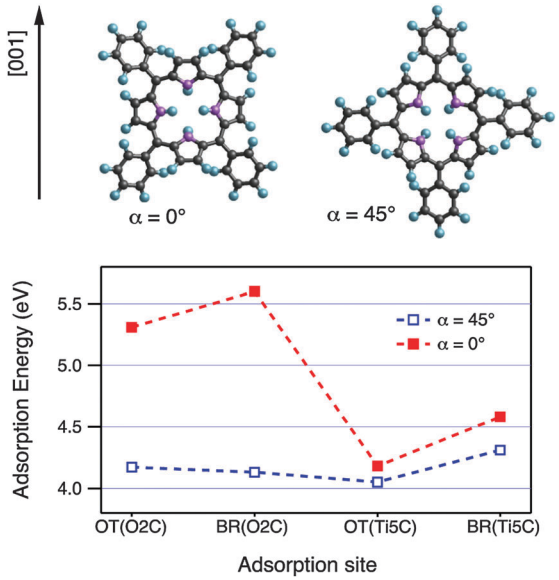

Fig. 4 Adsorption energy of 4*H*-TPP as a function of the adsorption site (on-top, OT, and bridge, BR) on the O^{2c}, and Ti^{5c} rows. The values have been computed for two different azimuthal orientations ($\alpha = 0°, 45°$) of the porphyrin macrocycle with respect to the substrate [001] direction, as sketched in the upper drawings.

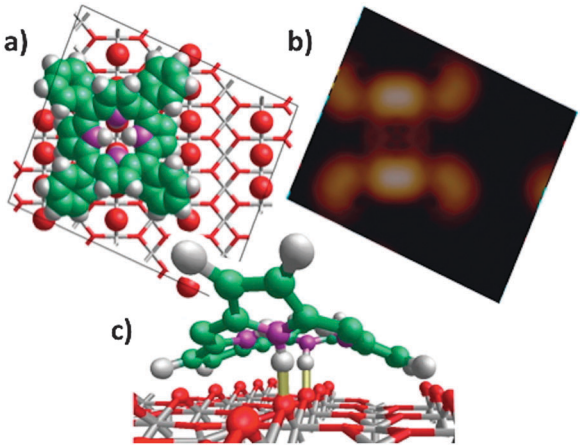

Fig. 5 The ball and stick model of the 4*H*-TPP adsorption configuration is shown in panel (a), where the adopted supercell is also sketched. The simulated STM images are shown in panel (b), whose saddle-shape molecular appearance is in excellent agreement with the observed one. The deformation of the adsorbate can be appreciated in the perspective view of panel (c), where the N–H$\cdots$O$_{br}$ hydrogen bonds are also highlighted as yellow sticks.

The topographic images calculated for 2*H*-TPP are very similar to those of 4*H*-TPP, where the main structural difference is found to be the average tilt angle of the pyrrolic rings that increases by 6° upon hydrogen uptake. This difference cannot be appreciated in our STM images (room temperature), but is consistent with the observed dichroism of the residual iminic component in the N K-edge NEXAFS, as compared to the pyrrolic one (see Fig. S2, ESI†). In this equilibrium configuration, the energy reaction of hydrogen uptake from the surface is much more exothermic (−1.40 eV) with respect to the gas-phase case (Table 1). It is worth noticing that, while the mechanism of hydrogen incorporation into bulk TiO_2 is controversial,[17,20] there is a general consensus about the interlayer H diffusion barrier calculated to be ∼1 eV for the TiO_2(110) planes,[21] which opens the way also to a possible mechanism of bulk hydrogen uptake.

DFT simulations of the N 1s photoemission peaks were performed using clusters extracted from the previously optimized slab models. These include the adsorbed species as well the relevant part of the first TiO_2 layer, and a convenient number of saturating hydrogen atoms. The results (reported in Table 2) reproduce quite well the observed core level shift (CLS) between the iminic and pyrrolic nitrogen of 2*H*-TPP. The uptake of two hydrogen atoms is expected to yield a small shift of ∼0.3 eV towards higher binding energy, BE, with respect to the pristine pyrrolic pair (which are coordinated to the oxygen atoms underneath). Such a small CLS is not resolved in our XPS measurements, nonetheless it is fully consistent with the broadening (ΔFWHM = +0.4 eV) of the main nitrogen component observed in the monolayer range with respect to the multilayer one (see peak analysis in Fig. S4, ESI†).

Table 2 N 1s binding energy and core level shift with respect to pyrrolic N

Molecule	Pyrrolic B.E. [eV]	Iminic CLS [eV]	Iminic + 2H CLS [eV]
2*H*-TPP multilayer	400.15 exp	−2.06 exp	—
2*H*-TPP ML	400.55 exp	−1.95[a] exp	—
2*H*-TPP gas	393.30 calc	−1.95 calc	—
2*H*-TPP ads	392.78 calc	−1.83 calc	—
4*H*-TPP ads	392.73 calc	—	+0.32 calc

[a] From the minority component of unreacted molecules.

Experimental and theoretical methods

Experimental details

We performed synchrotron radiation spectroscopy measurements at the ALOISA beamline[22a] of the Elettra Synchrotron (Trieste, Italy). We imaged the molecules using an Aarhus microscope (provided by SPECS) at the Centro de Fisica de Materiales (CSIC-UPV, San Sebastian, Spain), whose experimental chamber is also equipped with an XPS analyzer for checking the preparation of the molecular films.[4c]

All XPS measurements have been performed in transverse magnetic polarization (TM, *i.e.* close to p-polarization) and normal emission geometry, with the sample kept at a grazing angle of 4°. Spectra have been collected using a hemispherical electron spectrometer (mean radius 66 mm) equipped with a 2D delay-line detector. We measured the VB spectra at a photon energy of 140 eV with an overall energy resolution of ∼120 meV. We measured core level photoemission spectra of O 1s, Ti 2p, N 1s and C 1s with a photon energy of 650 and 500 eV at the corresponding overall resolution of 280 and 160 meV, respectively. We calibrated the photoemission spectra to the binding energy of Ti $2p_{3/2}$ = 459.1 eV and Ti 3p = 37.6 ± 0.05 eV.

We measured the NEXAFS spectra at the carbon and nitrogen K-edge by partial electron yield, using a channeltron equipped with a repeller grid kept at a negative bias in order to let the Auger electron of the corresponding ionization edge pass through. The photon energy resolution was set to ∼100 meV for both ionization thresholds. The orientation of the surface with respect to the photon beam polarization (linear) was changed from TM to transverse electric (TE, *i.e.* s-polarization) by rotation of the surface around the photon beam axis while keeping a constant grazing angle of 6°. Absolute calibration of the photon energy scale is performed *a posteriori* by using as a reference the carbon and nitrogen absorption features detected in the drain current recorded on the gold coating of the last beamline optics (synchronized acquisition). The scattering geometry of the ALOISA endstation as well as the absolute calibration procedure are described in more detail in ref. 22*b*.

We employed a number of different samples purchased from Mateck that were also exchanged between the ALOISA Synchrotron beamline and the STM apparatus. We followed the same preparation protocol for cleaning the surface: sputtering with Ar^+ at 800 eV followed by short annealing up to 1000 ± 50 K (1 min at maximum temperature), which yields dark blue samples. All the STM images were acquired at room temperature using a tungsten electrochemically etched tip. In both experimental apparatuses, we deposited molecules from boron nitride Knudsen cells at a typical temperature of 460 ± 10 K for

2*H*-OEP and 570 ± 10 K for both 2*H*-TPP and 2*H*-TBTPP. The corresponding deposition rate is found to be in the range of 0.1–0.5 Å min^{-1}, as monitored by room temperature quartz microbalances. In the ALOISA apparatus, the monolayer coverage has been defined by recording the XPS intensity after thermal desorption of a multilayer. All of the porphyrins have shown the saturation of the monolayer at an equivalent coverage of ~2.5 Å.

Computational details

Adsorption of 2*H*-TPP on the TiO_2(110) surface was studied with DFT calculations using the Quantum ESPRESSO package.[23a] The PBE functional[23b] in conjunction with Grimme dispersion corrections[23c,d] was used. Ion cores were described by Vanderbilt ultrasoft pseudopotentials (PPs), which included C, N, and O 1s orbitals. Ti ions were described either by "large core" PPs including 1s–3p electrons, or with "small cores", including 1s–2p electrons (see below). The kinetic energy cutoff of the planewave expansion was 25 Ry (200 Ry for the Vanderbilt augmentation charge).

To simulate low-coverage conditions, we adopted an oblique $\begin{pmatrix} \bar{3} & 3 \\ 6 & 1 \end{pmatrix}$ supercell including 21 unit cells. The theoretical PBE-D lattice constants of TiO_2 were used.[19] Because of the large size and conformational flexibility of the adsorbate, which requires both large memory usage and long run times, the energetics of the 2*H*-TPP/4*H*-TPP species with the TiO_2 surface was first explored on thin (three TiO_2 layers) slab models using "large core" PPs. The structure and the stability of the most favorable configurations were eventually recomputed more accurately using "small core" pseudopotentials and four TiO_2 layers. The two bottom layers of the slabs were frozen in the bulk structure. Because of the large size of the supercells, only the Γ point of the Brillouin zone was sampled.

We estimated the N 1s CLSs of the isolated 2*H*-TPP and the adsorbed 2*H*-TPP and 4*H*-TPP molecules by means of hybrid-DFT calculations, employing the PBE0 functional.[24] Calculations were carried out using the ADF code.[25] Wavefunctions were expanded over a TZP basis set of Slater-type orbitals. Inner electrons of Ti, O, and C up to the 3p, 1s and 1s levels, respectively, were treated as frozen cores, whereas all electrons pertaining to N atoms were allowed to relax. The scalar Zero Order Regular Approximation (ZORA) to the relativistic Hamiltonian was applied.[26] Molecular clusters cut out from the optimized slab and properly saturated with H atoms were used as models for adsorbed molecules. In both the 2*H*-TPP and the 4*H*-TPP cases, the surface was represented as a $Ti_{31}O_{92}H_{60}$ cluster.

Conclusions

In conclusion, our systematic study of metal-free porphyrins with different functional ends confirms that the TiO_2(110) substrate strongly favors the capture of surface hydrogen by tetrapyrrolic macrocycles, independent of the functional terminations. The energy gain associated with this chemical reaction is found to be larger than the barrier for hydrogen interlayer diffusion, which makes conceivable a hydrogen extraction path from the titania bulk. When comparing our systems with the case of phthalocyanines, one should consider the competitive reaction channel offered by the four additional meso-nitrogen atoms. In fact, upon hydrogen exposure, first layer MnPc molecules on Au(111) have been shown to dissociate and link two hydrogen atoms at opposite meso sites.[7] This reaction path might be enhanced at the TiO_2(110) surface, as observed for the porphyrin case, thus explaining the excess of pyrrolic nitrogen reported also for metalated species like FePc[12] and ZnPc.[14]

Acknowledgements

We acknowledge support from the MIUR of Italy through PRIN project DESCARTES (no. 2010BNZ3F2), and by CINECA (ISCRA-B project E-TROPPO), from the Spanish Government (Grant MAT2013-46593-C6-4-P) and from the Basque Department of Education (Grant IT-621-13). M.A. is also grateful for financial support from DIPC.

Notes and references

1 W. Auwärter, D. Ecija, F. Klappenberger and J. V. Barth, *Nat. Chem.*, 2015, **7**, 105.

2 (*a*) J. Miguel, C. F. Hermanns, M. Bernien, A. Krüger and W. Kuch, *J. Phys. Chem. Lett.*, 2011, **2**, 1455; (*b*) C. Krull, R. Robles, A. Mugarza and P. Gambardella, *Nat. Mater.*, 2013, **12**, 337; (*c*) S. Vijayaraghavan, W. Auwärter, D. Acija, K. Seufert, S. Rusponi, T. Houwaart, P. Sautet, M.-L. Bocquet, P. Thakur, S. Stepanow, U. Schlickum, M. Etzkorn, H. Brune and J. V. Barth, *ACS Nano*, 2015, **9**, 3605.

3 (*a*) F. Sedona, M. Di Marion, D. Forrer, A. Vittadini, M. Casarin, A. Cossaro, L. Floreano, A. Verdini and M. Sambi, *Nat. Mater.*, 2012, **11**, 970; (*b*) B. E. Murphy, S. A. Krasnikov, N. N. Sergeeva, A. A. Cafolla, A. B. Preobrajenski, A. N. Chaika, O. Lübben and I. V. Shvets, *ACS Nano*, 2014, **8**, 5190; (*c*) D. A. Duncan, P. S. Deimel, A. Wiengarten, R. Han, R. G. Acres, W. Auwarter, P. Feulner, A. C. Papageorgiou, F. Allegretti and J. V. Barth, *Chem. Commun.*, 2015, **51**, 9483.

4 (*a*) R. Gonzalez-Moreno, C. Sanchez-Sanchez, M. Trelka, R. Otero, A. Cossaro, A. Verdini, L. Floreano, M. Ruiz-Bermejo, A. Garcia-Lekue, J. A. Martin-Gago and C. Rogero, *J. Phys. Chem. C*, 2011, **115**, 6849; (*b*) A. Goldoni, C. A. Pignedoli, G. Di Santo, C. Castellarin-Cudia, E. Magnano, F. Bondino, A. Verdini and D. Passerone, *ACS Nano*, 2012, **12**, 10800; (*c*) M. Abadia, R. Gonzalez-Moreno, A. Sarasola, G. Otero-Irureta, A. Verdini, L. Floreano, A. Garcia-Lekue and C. Rogero, *J. Phys. Chem. C*, 2014, **118**, 29704; (*d*) M. Stark, S. Ditze, M. Lepper, L. Zhang, H. Schlott, F. Buchner, M. Röckert, M. Chen, O. Lytken, H.-P. Steinrück and H. Marbach, *Chem. Commun.*, 2014, **50**, 10225; (*e*) J. Mielke, F. Hanke, M. V. Peters, S. Hecht, M. Persson and L. Grill, *J. Am. Chem. Soc.*, 2015, **137**, 1844.

5 (*a*) W. Auwärter, A. Weber-Bargioni, S. Brink, A. Riemann, A. Schiffrin, M. Ruben and J. V. Barth, *ChemPhysChem*, 2007, **8**, 250; (*b*) G. Di Santo, C. Castellarin-Cudia, M. Fanetti, B. Taleatu, P. Borghetti, L. Sangaletti, L. Floreano, E. Magnano, F. Bondino and A. Goldoni, *J. Phys. Chem. C*, 2011, **115**, 4155;

(*c*) C. Wang, Q. Fan, S. Hu, H. Ju, X. Feng, Y. Han, H. Pan, J. Zhu and J. M. Gottfried, *Chem. Commun.*, 2014, **50**, 8291.
6 W. Auwärter, K. Seufert, F. Bischoff, D. Ecija, S. Vijayaraghavan, S. Joshi, F. Klappenberger, N. Samudrala and J. V. Barth, *Nat. Nanotechnol.*, 2012, **7**, 41.
7 K. Yang, L. Liu, L. Zhang, W. Xiao, X. Fei, H. Chen, S. Du, K.-H. Ernst and H.-J. Gao, *ACS Nano*, 2014, **8**, 2246.
8 P. Palmgren, B. R. Priya, N. P. P. Niraj and M. Göthelid, *Sol. Energy Mater. Sol. Cells*, 2006, **90**, 3602.
9 N. Ishida and D. J. Fujita, *J. Phys. Chem. C*, 2012, **116**, 20300.
10 S. Verma and H. N. Ghosh, *J. Phys. Chem. Lett.*, 2012, **3**, 1877.
11 G. Mattioli, F. Filippone, P. Giannozzi, R. Caminiti and A. A. Bonapasta, *Chem. Mater.*, 2009, **21**, 4555.
12 P. Palmgren, K. Nilson, S. Yu, F. Hennies, T. Angot, C. I. Nlebedim, J.-M. Layet, G. Le Lay and M. Göthelid, *J. Phys. Chem. C*, 2008, **112**, 5972.
13 A. Rienzo, L. C. Mayor, G. Magnano, C. J. Satterley, E. Ataman, J. Schnadt, K. Schulte and J. N. O'Shea, *J. Chem. Phys.*, 2010, **132**, 084703.
14 S. Yu, S. Ahmadi, C. Sun, P. T. Z. Adibi, W. Chow, A. Pietzsch and M. Göthelid, *J. Chem. Phys.*, 2012, **136**, 154703.
15 P. Borghetti, G. Di Santo, C. Castellarin-Cudia, M. Fanetti, L. Sangaletti, E. Magnano, F. Bondino and A. Goldoni, *J. Chem. Phys.*, 2013, **138**, 1444702.
16 (*a*) O. W. Johnson, J. DeFord and J. W. Shaner, *J. Appl. Phys.*, 1973, **44**, 3008; (*b*) O. W. Johnson, S.-H. Paek and J. DeFord, *J. Appl. Phys.*, 1975, **46**, 1026; (*c*) Y. Chen, R. Gonzalez and K. L. Tsang, *Phys. Rev. Lett.*, 1984, **53**, 1077; (*d*) P. M. Kowalski, B. Meyer and D. Marx, *Phys. Rev. B: Condens. Matter Mater. Phys.*, 2009, **79**, 115410.
17 X.-L. Yin, M. Calatayud, H. Qiu, Y. Wang, A. Birkner, C. Minot and Ch. Wöll, *ChemPhysChem*, 2008, **9**, 253.
18 L. E. Walle, A. Borg, P. Uvdal and A. Sandell, *Phys. Rev. B: Condens. Matter Mater. Phys.*, 2009, **80**, 235436.
19 D. Forrer and A. Vittadini, *Chem. Phys. Lett.*, 2011, **516**, 72.
20 (*a*) M. Calatayud, X.-L. Yin, H. Qiu, Y. Wang, A. Birkner, C. Minot and Ch. Wöll, *Phys. Rev. Lett.*, 2010, **104**, 119603; (*b*) G. H. Enevoldsen, H. P. Pinto, A. S. Foster, M. C. R. Jensen, W. A. Hofer, B. Hammer, J. V. Lauritsen and F. Besenbacher, *Phys. Rev. Lett.*, 2010, **104**, 119604.
21 Y. Du, N. G. Petrik, N. A. Deskins, Z. Wang, M. A. Henderon, G. A. Kimmel and I. Lyubinetsky, *Phys. Chem. Chem. Phys.*, 2012, **14**, 3066.
22 (*a*) L. Floreano, G. Naletto, D. Cvetko, R. Gotter, M. Malvezzi, L. Marassi, A. Morgante, A. Santaniello, A. Verdini, F. Tommasini and G. Tondello, *Rev. Sci. Instrum.*, 1999, **70**, 3855; (*b*) L. Floreano, A. Cossaro, R. Gotter, A. Verdini, G. Bavdek, F. Evangelista, A. Ruocco, A. Morgante and D. Cvetko, *J. Phys. Chem. C*, 2008, **112**, 10794.
23 (*a*) P. Giannozzi, *et al.*, *J. Phys.: Condens. Matter*, 2009, **21**, 395502; (*b*) J. Perdew, K. Burke and M. Enzerhof, *Phys. Rev. Lett.*, 1996, **77**, 3865; (*c*) S. Grimme, *J. Comput. Chem.*, 2006, **27**, 1787; (*d*) V. Barone, M. Casarin, D. Forrer, M. Pavone, M. Sambi and A. Vittadini, *J. Comput. Chem.*, 2009, **30**, 934.
24 C. Adamo and V. Barone, *J. Chem. Phys.*, 1999, **110**, 6158.
25 Amsterdam Density Functional v. 2014 http://www.scm.com/ADF.
26 (*a*) E. van Lenthe, E. J. Baerends and J. G. Snijders, *J. Chem. Phys.*, 1993, **99**, 4597; (*b*) E. van Lenthe, E. J. Baerends and J. G. Snijders, *J. Chem. Phys.*, 1994, **101**, 9783.

